Image resolution depending on slab thickness and object distance in a two-dimensional photonic-crystal-based superlens

Xiangdong Zhang
Department of Physics, Beijing Normal University, Beijing 100875, People's Republic of China
(Received 26 June 2004; published 15 November 2004)

Based on the exact numerical simulation and physical analysis, we have demonstrated all-angle single-beam left-handed behavior and superlens for both transverse electric and transverse magnetic modes in a two-dimensional coated photonic crystal. The imaging behaviors by two-dimensional photonic-crystal-based superlens have been investigated systematically. Good-quality images and focusing, with relative refractive index of −1, have been observed in these systems for both polarized waves. In contrast to the images in near-field region for the lowest valence band, non-near-field images, explicitly following the well-known wave-beam negative refraction law, have been demonstrated. The absorption and compensation for the losses by introducing optical gain in these systems have also been discussed. Thus, extensive applications of such a phenomenon to optical devices are anticipated.

DOI: 10.1103/PhysRevB.70.195110 PACS number(s): 78.20.Ci, 42.70.Qs, 41.20.Jb, 42.30.Wb

I. INTRODUCTION

Recently there has been a great deal of interest in studying a class of media that has become known as the left-handed materials (LHMs).[1–20] These materials are characterized by simultaneous negative permittivity ϵ and negative permeability μ. Properties of such materials were analyzed theoretically by Veselago over 30 years ago.[1] As was shown by Veselago, the LHMs possess some peculiar electromagnetic properties such as inverse Snell's law, reversed Doppler shift, and reversed Cherenkov radiation. It had also been suggested that a slab of the LHM could be employed as an unconventional flat lens.

Due to the absence of naturally occurring materials having both negative ϵ and negative μ, Veselago's prediction did not receive much attention until recently, when a system consisting of an array of split-ring resonators and metallic wires was prepared and demonstrated to have negative refractive index experimentally.[3,4] Subsequently, some physical properties of the LHMs were analyzed by many authors.[5–20] Pendry[5] predicted that the LHM slab can amplify the evanescent waves and the flat lens constructed from such a material with $\epsilon=\mu=-1$ could in principle work as "perfect" lens (superlens). Although the concept of superlens was questioned by a number of authors,[21] more detailed physical considerations had shown that the construction of an "almost perfect" lens is indeed possible.[22–27] Recently, such image behaviors have been observed by some numerical simulations[22–24] and experimental measurements.[24–27] However, only near-field images were demonstrated and extensive applications of such a phenomenon were limited.[22–27]

It was shown that negative refraction could also occur in photonic crystal (PC).[28–39] The physical principles that allow negative refraction in them arise from the dispersion characteristics of wave propagation in a periodic medium, which can well be described by analyzing the equifrequency surface (EFS) of the band structures.[28–37] In the PC structures, there are two kinds of cases for negative refraction occurring.[31] The first is the left-handed behavior as being described earlier.[29–32] In this case, **k**, **E**, and **H** form a left-handed set of vectors (i.e., $\mathbf{S}\cdot\mathbf{k}<0$, where **S** is the Poynting vectors). Another case is that the negative refraction can be realized without employing a negative index or a backward wave effect.[33–37] In this case, the PC is behaving much like a uniform right-handed medium (i.e., $\mathbf{S}\cdot\mathbf{k}>0$). Recently, Luo *et al.*[33] have shown that all-angle negative refraction could be achieved at the lowest band of two-dimensional (2D) PC in the case of $\mathbf{S}\cdot\mathbf{k}>0$. The advantages of the negative refraction in the lowest valence band are single-mode and high transmission. These can help us to design microsuperlens and realize the focusing of the wave. Very recently, the subwavelength focusing and image by 2D PC slab have been observed experimentally.[34–36] Absolute negative refraction and imaging of unpolarized electromagnetic wave by 2D PC slabs have also been obtained.[37] However, due to the anisotropy of dispersion in 2D PC, such images only appear in near-field region.[38,39]

How to realize a good-quality non-near-field image becomes an important issue. The prerequisite condition to realize such a phenomenon is the negative refraction which possesses the single-mode and high transmission. Although some works[29] have shown that the left-hand behavior and focusing exist in the 2D PC, the multiple-mode and low transmission in high frequencies affect the features of focusing.[31,32] It is well known that the electromagnetic (EM) wave can be decomposed into transverse magnetic (TM) modes (S wave) and transverse electric (TE) modes (P wave) for the 2D PC structures.[40] However, the investigations[29] have shown that air-hole-type 2D PCs possess good left-handed behavior for TM modes, and a pillar type 2D PC prefers TE modes. In this paper, we will demonstrate that coated cylinder PCs with triangular lattice posses double features. They have not only good left-handed behavior for the TM modes, but also for the TE modes. Most interestingly, the all-angle single-beam left-handed behaviors with relative refractive index of −1 for both polarized waves have been found in these systems. Thus, high-quality focusing and imaging behavior have been obtained. In contrast to the images

in the near-field region for the lowest valence band, non-near-field images, explicitly following the well-known wave-beam negative refraction law, have been demonstrated. The absorption and compensation for the losses by introducing optical gain in these systems have also been discussed.

The rest of this paper is arranged as follows. In Sec. II, we demonstrate the all-angle single-beam left-handed behaviors for both TE and TM modes in a two-dimensional coated photonic crystals. The good-quality non-near-field imaging behaviors are discussed in Sec. III. In Sec. IV, we analyze the effect of absorption and gain. The conclusions are given in Sec. V.

II. LEFT-HANDED BEHAVIOR IN 2D COATED CYLINDER PC

We consider a 2D triangular lattice of coated cylinders immersed in an air background with lattice constant a. The coated cylinders have metallic cores coated with a dielectric coating. The radii of metallic core and coated cylinder are $0.25a$ and $0.45a$, respectively. The dielectric constants of dielectric coating are taken as 11.4 for the S wave and 7.0 for the P wave. For the metallic component, we use the frequency-dependent dielectric constant,[41]

$$\epsilon = 1 - \frac{f_p^2}{f(f + i\gamma)}, \tag{1}$$

where f_p and γ are the plasma frequency and the absorption coefficient. Following Ref. 41, for all numerical calculations carried out in this work, we have chosen $f_p = 3600$ THz and $\gamma = 340$ THz, which corresponds to a conductivity close to that of Ti. However, our discussion and conclusions given later can apply to other metal parameters as well. In order to simplify the problem, we first consider the cases without absorption ($\gamma = 0$). The effect of absorption will be discussed at the latter part.

For all calculations throughout this paper, we adopt the multiple-scattering Korringa-Kohn-Rostoker method[42] as our main computational tool, both to calculate the photonic band structure in the reciprocal space and to perform numerical simulations for wave propagating in the finite real space. The multiple-scattering method is not only success in the calculations of band structure, it is also best suited for a finite collection of cylinders with a continuous incident wave of fixed frequency. For circular cylinders, the scattering property of the individual cylinder can be obtained analytically, relating the scattered fields to the incident fields. The total field, which includes the incident plus the multiple-scattered field, can then be obtained by solving a linear system of equations, whose size is proportional to the number of cylinders in the system. Both near-field and far-field radiation patterns can be obtained straightforwardly. So, such a method is a very efficient way of handling the scattering problem of a finite sample containing cylinders of circular cross sections, and it is capable of reproducing accurately the experimental transmission data, which should be regarded as exact numerical simulation. The detailed description of this method has been given in Ref. 42.

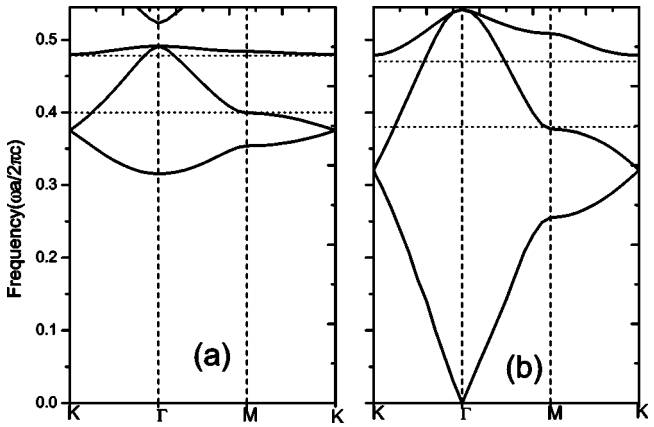

FIG. 1. The calculated photonic band structures of a triangular lattice of coated cylinder in air for the S wave (a) and P wave (b). The radii of the dielectric cylinder and inner metallic cylinder are $R = 0.45a$ and $r = 0.25a$, respectively. Here $a = 3$ mm. The dielectric constants are $\epsilon = 11.4$ for the S wave and $\epsilon = 7$ for the P wave. Dotted lines mark the region for negative refraction.

The calculated results of band structure for the S wave and the P wave are plotted in Figs. 1(a) and 1(b), respectively. We focus on the problems of wave propagation in the second bands marked by dotted lines in Figs. 1(a) and 1(b). Owing to the strong scattering effects, it is generally difficult to describe the propagation behavior of EM wave in the PC in a simple yet accurate way. However, a lot of theoretical and experimental practices[28–39] have shown that the overall behavior of the wave propagation within a PC can be well described by analyzing the EFS of the band structures, because the gradient vectors of constant-frequency contours in k space give the group velocities of the photonic modes. Thus, the propagation direction of energy velocity of EM wave can be deduced from them. The EFS contours of the earlier system for the S wave and the P wave at several relevant frequencies are demonstrated in Figs. 2(a) and 2(b), respectively.

It is clear from the figures that some EFS contours such as $\omega = 0.42 - 0.47(2\pi c/a)$ for the S wave and the P wave are very close to a perfect circle, indicating that the crystal can be regarded as an effective homogeneous medium at these frequencies. At the same time, we also notice that the frequencies increase inwards for both cases, meaning that $\mathbf{S} \cdot \mathbf{k}_i < 0$ and the group velocities (v_g) are opposite to the phase velocity. Here, $\mathbf{S}$ and $\mathbf{k}_i$ represent the Poynting vector and wave vector, respectively. These indicate that the transmitting features of the wave in the earlier PC structures are the left-handed behavior. The conservation of the surface-parallel wave vector would result in the negative refraction effect in these cases, which the direction of the refracted wave inside the PC can also be estimated from the EFS. Then, we apply Snell's law in these cases, the negative indexes of refraction can also be obtained. Figures 3(a) and 3(b) show the negative effective indexes as function of frequencies for the S wave and the P wave, respectively. It is interesting that the cases with relative refractive index of -1 for the S wave at $\omega = 0.42(2\pi c/a)$ and the P wave at $\omega = 0.43(2\pi c/a)$ have been found.

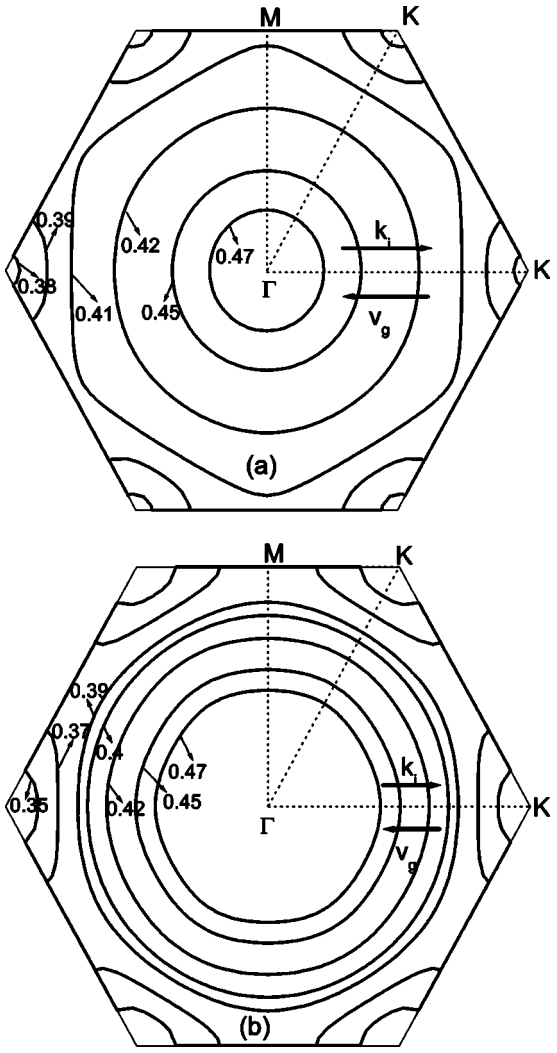

FIG. 2. Several constant-frequency contours for the S wave (a) and P wave (b) of the second band of the 2D PCs which are corresponded to the cases in Figs. 1(a) and 1(b), respectively. The numbers in the figure mark the frequencies in unit of $2\pi c/a$. k_i and v_g represent the wave vector and the group velocity, respectively.

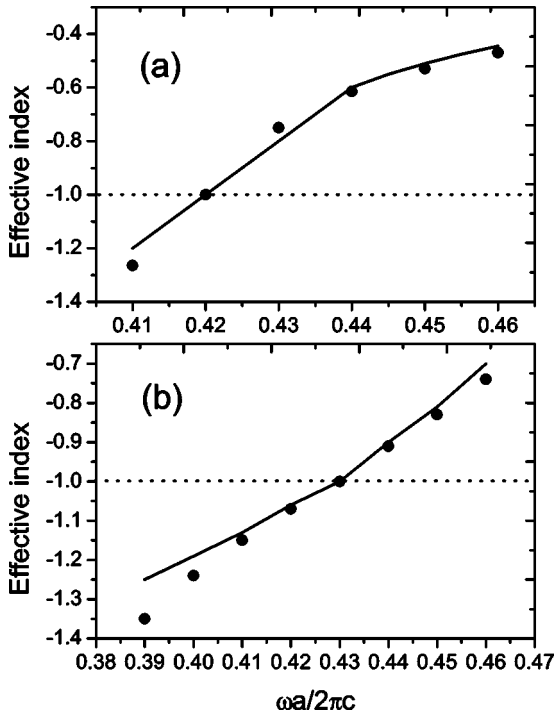

FIG. 3. Effective indexes vs frequencies for the S wave (a) and P wave (b). The crystals and parameters are identical to those in Fig. 1. The positions of relative refractive index of −1 are marked by dotted lines.

In order to test the above analysis, we do numerical simulations in the present systems. We take the slab samples which consist of 13-layer coated cylinders in the air background with a triangular arrays. The surface normal of the PC slab is along ΓK direction. The parameters of coated cylinders are the same to the cases in Fig. 1. When a slit beam with a half width $2a$ goes through the slab material, it will be refracted two times by two interfaces of the slab. The shape of the sample and a snapshot of the refracted process are shown on the top of Fig. 4. There are different ray traces for the wave transmitting through the slab sample with various effective indexes, when the wave does not incident on the interface with normal direction. From the ray traces, we can deduce the effective refraction index of the slab material.

The simulations are based on a highly efficient and accurate multiple-scattering method.[42] In our calculations, the widths of the samples taken are large enough, such as $40a$, to avoid the edge diffraction effects. The calculated results for the S wave and the P wave are plotted in Figs. 4(a) and 4(b), respectively. The field energy patterns of incidence and refraction are shown in the figures. The arrows and texts illustrate the various beam directions. The geometries of the slab are also displayed. It can be clearly seen that the energy fluxes of refraction wave travel following the negative refraction law for both polarized waves. The negative refraction indexes for the S wave and the P wave obtained from the exact numerical simulation are marked as dark dots in Figs. 3(a) and 3(b), respectively. Comparing them with the estimated results [solid lines in Figs. 3(a) and 3(b)] from the EFS we find that the agreements between them are well around the region of effective refractive index of −1 for both polarized waves. When the effective refractive indexes deviate largely from −1, some differences can be found. This is due to the Goos-Hanchen effect, which had been discussed in Ref. 43.

Varying the angle of inclination of the sample, we have checked the cases with various incident angles. The calculated and analytical results of refracted angle θ versus incident angle θ_0 at $\omega=0.42(2\pi c/a)$ for the S wave and $\omega=0.43(2\pi c/a)$ for the P wave are summarized in Fig. 5 by the circle and triangular dark dots, respectively. Because the frequencies are below $0.5(2\pi c/a)$, all-angle single-beam negative refractions have been observed at these frequencies. More interestingly, θ is linearly proportional to θ_0 in the whole angle region for both polarized waves. This feature is close to the ideal LHM system that can serve as a perfect superlens.[5]

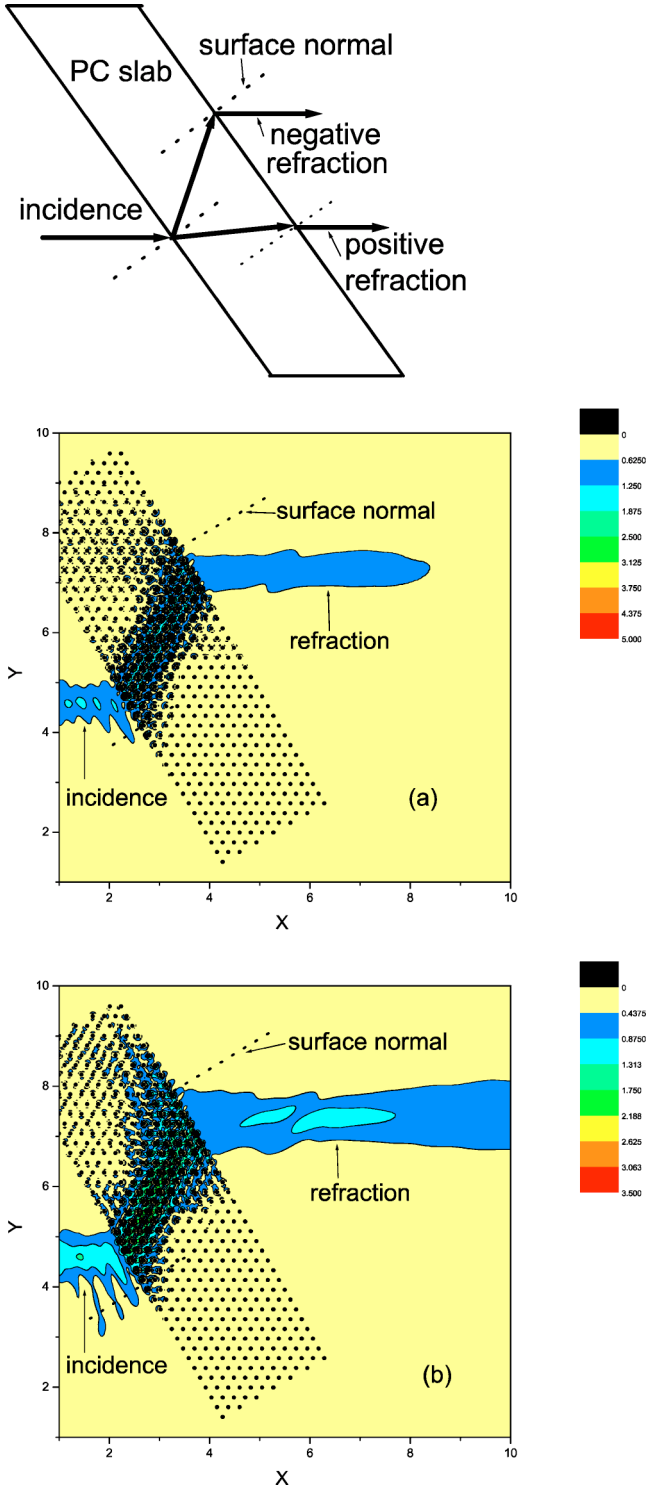

FIG. 4. (Color online) Simulation of negative refraction. The shape of the sample and a snapshot of refraction process are shown on top of the figure. The intensities of electric field for S wave (a) and magnetic field for P wave (b) for incidence and refraction are shown. The 2D PC slabs with 13 layers are marked as dark dots in figures. The frequencies of incident wave are $\omega=0.42(2\pi c/a)$ for the S wave and $\omega=0.43(2\pi c/a)$ for the P wave. The crystals and parameters in (a) and (b) are corresponded to those in Figs. 1(a) and 1(b), respectively.

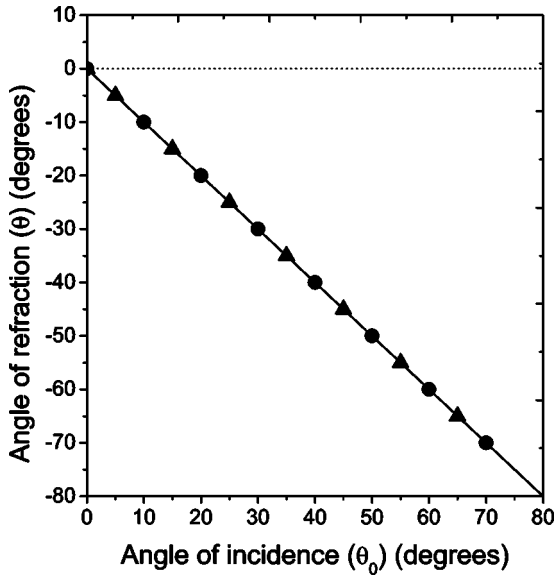

FIG. 5. The angles of refraction (θ) vs angles of incidence (θ_0) at $\omega=0.42(2\pi c/a)$ for the S wave and $\omega=0.43(2\pi c/a)$ for the P wave. Circle dots are corresponded to the S wave and triangular dots to the P wave.

III. IMAGE DEPENDING ON SLAB THICKNESS AND OBJECT DISTANCE

It is well known that an important application of negative refraction materials is the microsuperlens.[5] Ideally, such a superlens can focus a point source on one side of the lens into a real point image on the other side even for the case of a parallel sided slab of material. It possesses some advantages over conventional lenses. For example, it can break through the traditional limitation on lens performance and focus light on to an area smaller than a square wavelength.

In order to model such a superlens, we take a slab sample with $40a$ width and $11a$ thickness. A continuous-wave point source is placed at a distance $5.5a$ (half thickness of the sample) from the left surface of the slab. We first discuss the case for the point source of the S wave. The frequency of the incident wave emitting from such a point source is $0.42(2\pi c/a)$, which is corresponded to the case with relative refractive index of -1. If the wave transmits in such a 2D PC slab according to the well-known wave-beam refraction law, one should observe the focusing point in the middle of the slab and the image at the symmetric position in the opposite side of the slab, as being depicted by the simple picture on the top of Fig. 6.

To see whether or not such a phenomenon exists, we employ the multiple-scattering method[42] to calculate the propagation of waves in such a system. A typical field intensity pattern for the S wave across the above slab sample is plotted in Fig. 6(b). X and Y present vertical and transverse direction of wave propagating, respectively. The field intensity in the figure is over $30a\times 30a$ region around the center of the sample. The geometry of the PC slab is also displayed for clarity of view. The high quality image in the opposite side of the slab and the focusing in the middle of the slab according to the wave-beam refraction law are observed clearly. A

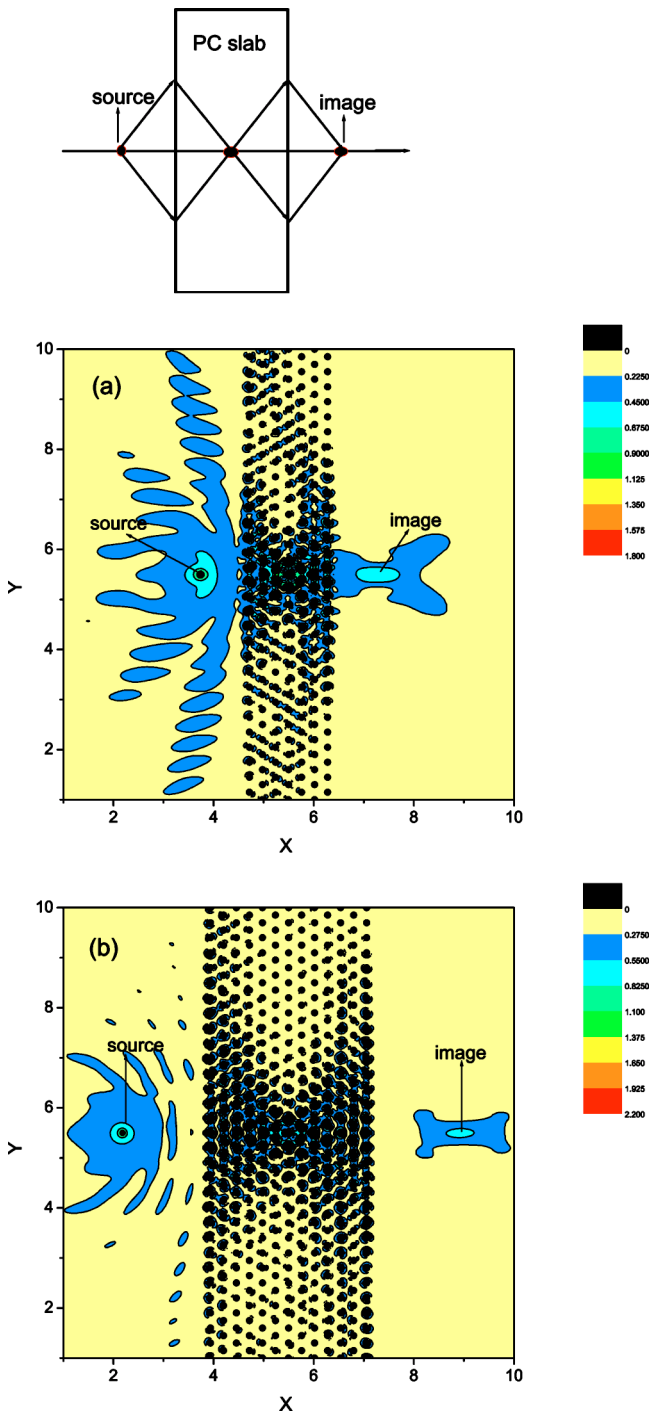

FIG. 6. (Color online) (a) The intensity distributions of point source and its image across a $7a$ 2D PC slab at frequency $\omega = 0.42(2\pi c/a)$ for the S wave. (b) The corresponding case for a slab with $11a$ thickness. Schematic picture depicting the lensing of a source by a PC slab to an image are shown on top of the figure.

closer look at the data reveals a transverse size (full size at half maximum) of the image spot as $0.7a$ (or 0.3λ), which is well below the conventional diffraction limit.

In order to clarify the sample thickness dependence of the image and focusing, we have also checked a series of slab samples with various thickness. Similar phenomena have also been observed. For example, Fig. 6(a) shows the calcu-

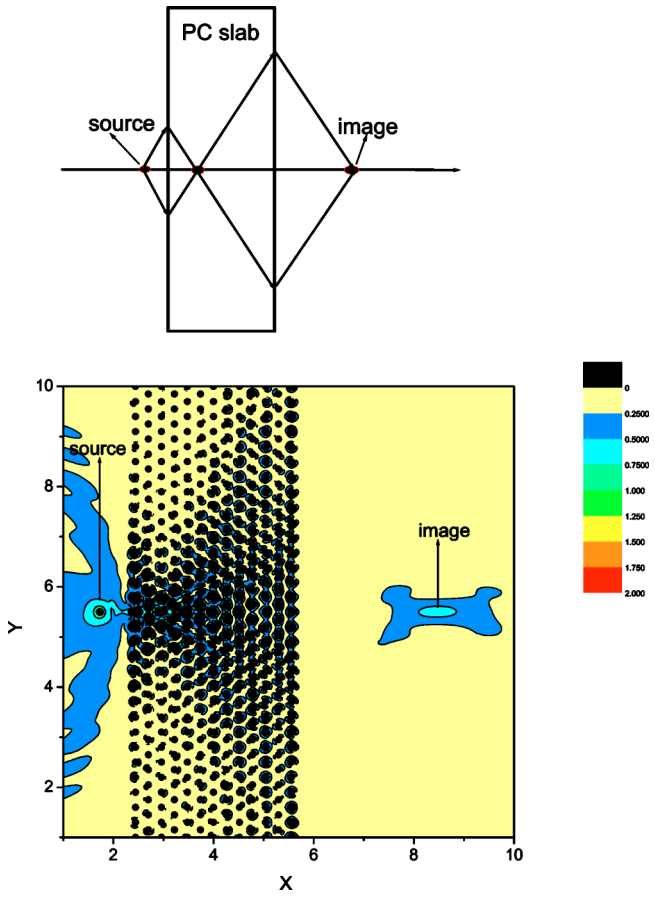

FIG. 7. (Color online) The intensity distributions of point source and its image across a $11a$ 2D PC slab at frequency $\omega = 0.42(2\pi c/a)$ for the S wave. The point source is placed at $2a$ distance from the left surface of the slab. Schematic picture depicting the lensing of a point source by a PC slab to an image are shown on top of the figure.

lated field energy pattern for a $7a$ thick sample. A monochromatic point source with $\omega = 0.42(2\pi c/a)$ is placed at a distance of half thickness of the sample $(3.5a)$ from the left surface of the slab and its image is found again near the symmetric position in the opposite side of the slab.

To have a more complete vision on the imaging effect of this type of superlens, we move the light source and see what happens to the imaging behavior. We first put a point source near the left surface of the slab. In this case, the refracted process following wave-beam negative refraction law is shown on the top of Fig. 7. The calculated intensity distribution is plotted in Fig. 7. In our simulations, the point source is placed at a distance of $2.0a$ from the left surface of the sample and the image is found near $9a$ from the right surface. The excellent agreements between the simulations and the estimated results from the rules of geometric optics are obvious. The corresponded result that a point source is far from the left surface is displayed in Fig. 8. In this case, the point source is placed at a distance of $9.0a$ from the left surface of the sample and the image is found near $2a$ from the right surface. Comparing the simulations with the snapshot of refracted process according to the wave-beam nega-

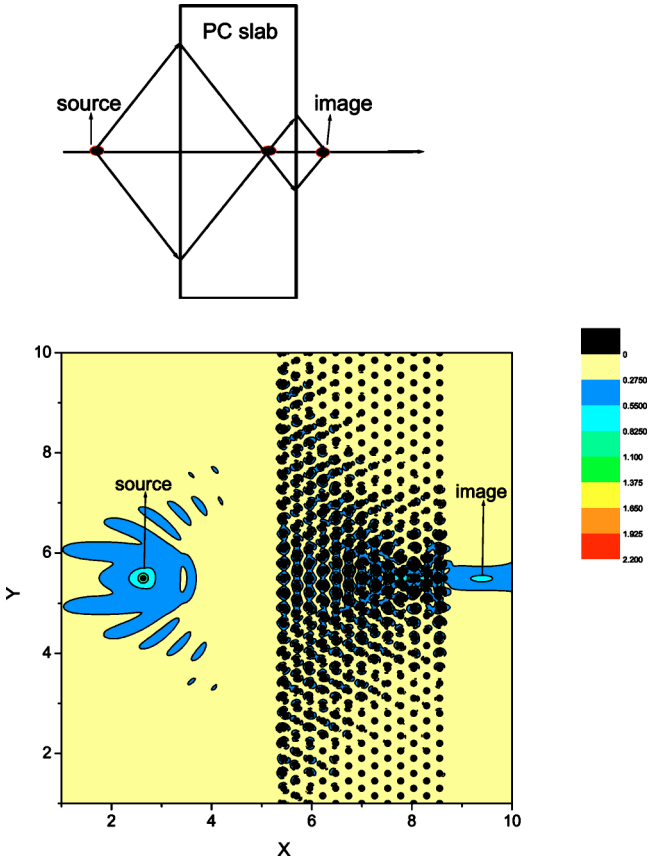

FIG. 8. (Color online) The intensity distributions of point source and its image across a $11a$ 2D PC slab at frequency $\omega = 0.42(2\pi c/a)$ for the S wave. The point source is placed at $9a$ distance from the left surface of the slab. Schematic picture depicting the lensing of a point source by a PC slab to an image are shown on top of the figure.

tive refraction law shown on the top of Fig. 8, we again find the excellent agreements between them.

The earlier results are only for the S wave, in the following, we will investigate the case of the P wave. We take the PC slab samples with $40a$ width and various thicknesses. A point source of the P wave is placed at a distance of half thickness of the sample from the left surface of the slab. The frequency of the incident wave emitting from such a point source is $0.43(2\pi c/a)$, which is corresponded to the case with relative refractive index of -1 for the P wave. The propagation behaviors of the P waves in such systems are still calculated by the multiple-scattering method.[42] Figures 9(a) and 9(b) show the cases with $7a$ and $13a$ thick slab, respectively. Similar features to Fig. 7 for the S wave are found. If we move the source position, the effect of source position on the image for the P wave can also be checked. The calculated results under two kinds of source position for the P wave are plotted in Figs. 10(a) and 10(b), respectively. The cases for the P waves are similar to those of the S waves in Fig. 8.

These observations indicate clearly that the imaging behaviors depend on the slab thickness and the object distance, explicitly following the well-known wave-beam negative refraction law. Therefore, such PC slabs in some frequencies

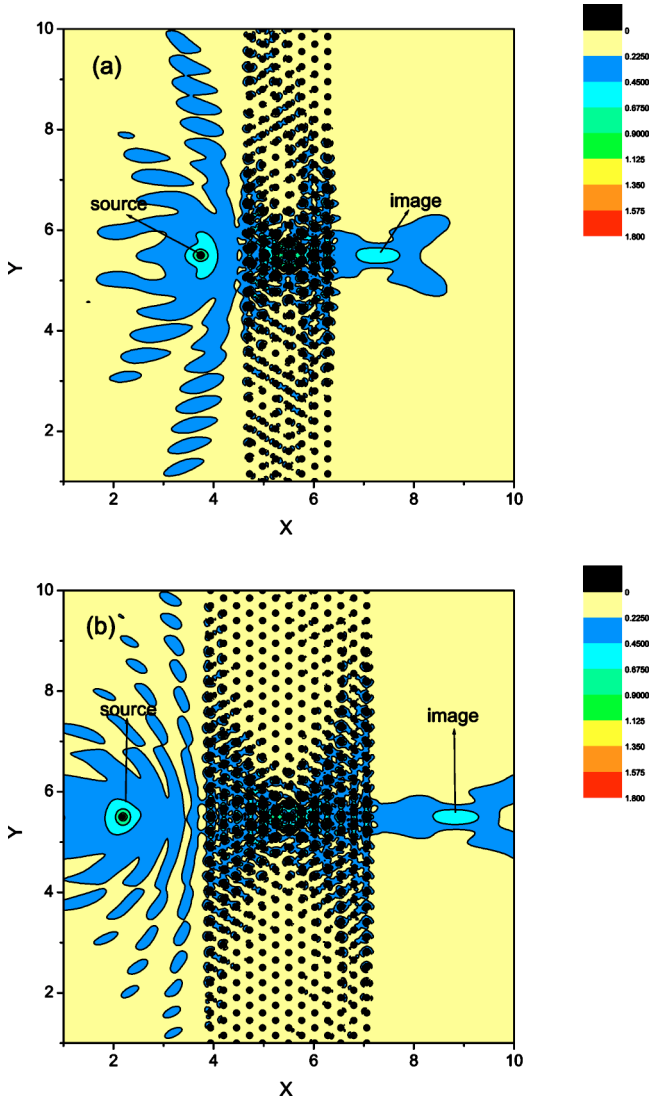

FIG. 9. (Color online) (a) The intensity distribution of point source and its image across a $7a$ 2D PC slab at frequency $\omega = 0.43(2\pi c/a)$ for the P wave. (b) The corresponding case for a slab with $11a$ thickness. The point source is placed at a distance with half thickness of the sample from the left surface of the slab.

can be considered as homogeneous effective medium with effective refraction index of -1. The high-quality focusing and images can be realized in these PC systems for both the S wave and P wave.

IV. EFFECT OF ABSORPTION AND GAIN

The earlier investigations have shown that the PC slab consisting of coated cylinders is actually considered as a good superlens for both polarized waves. The common features of these coated systems are that they all include metal components. Therefore, the absorption for these systems is inevitable. Lou *et al.*[38] have pointed that the central image peak disappear and the image degrade gradually with the increase of absorption. However, fortunately, the loss can be overcome by introducing the optical gain in the systems.

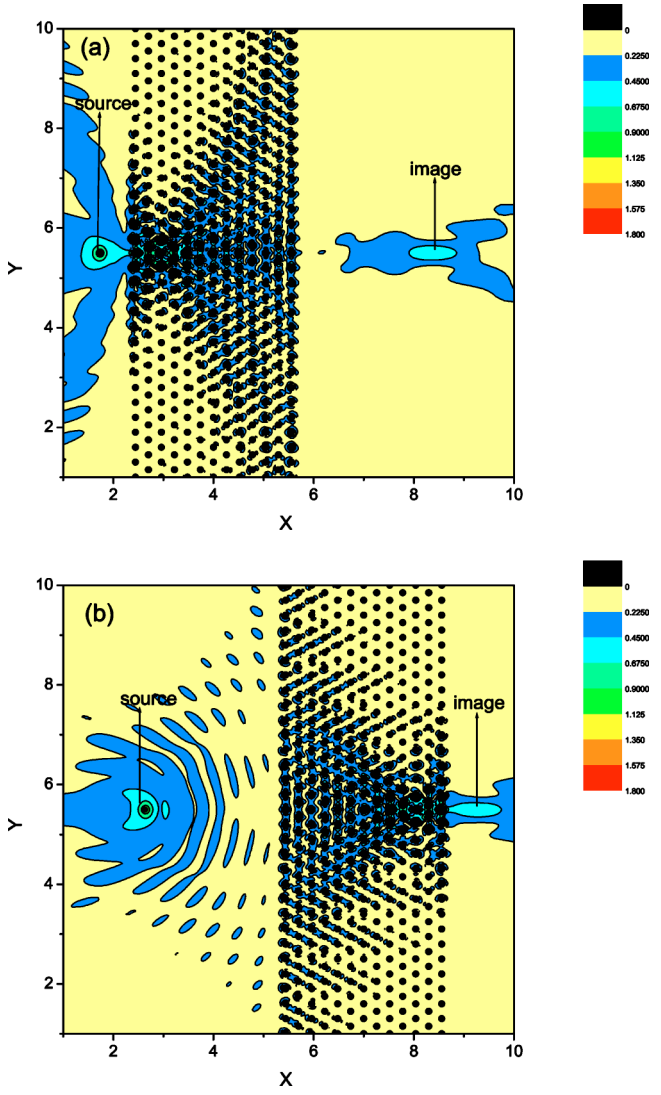

FIG. 10. (Color online) The intensity distribution of point source and its image across a $11a$ 2D PC slab at frequency $\omega = 0.43(2\pi c/a)$ for the P wave. (a) and (b) represent the cases with different source positions, $2a$ and $9a$ distances from the left surface of the slab, respectively.

Recently, Ramakrishna and Pendry[19] have suggested a method to remove the absorption by introducing optical gain into the lens made from a multilayers stack of thin alternating layers of silver and dielectric medium. Here, we borrow their idea and introduce the optical gain in the 2D PC superlens.

Figure 11(a) shows the intensity distribution as a function of transverse coordinate (y/a) for the S wave at the image plane ($5.5a$ away from the second interface). Curve A is corresponded to the perfect case without absorption and curve B to that with absorption, in this case γ is taken as 340 THz. Comparing curve A with curve B, we find that the central peak of image decrease with the introducing of absorption, which agrees with the analysis of Ref. 38. This is also consistent with the numerical studies of left-handed structures constructed from split-ring resonators in Refs. 7 and 8. The result by introducing gain to remove the absorption for the corresponding case is plotted in Fig. 11(b). Curves B in Figs. 11(a) and 11(b) are the same one, and curve C in Fig. 11(b) is the result with the dielectric constant $\epsilon = 11.4 - 0.08i$ for the dielectric part of coated cylinder. We do not find any difference between curve A in Fig. 11(a) and curve C in Fig. 11(b).

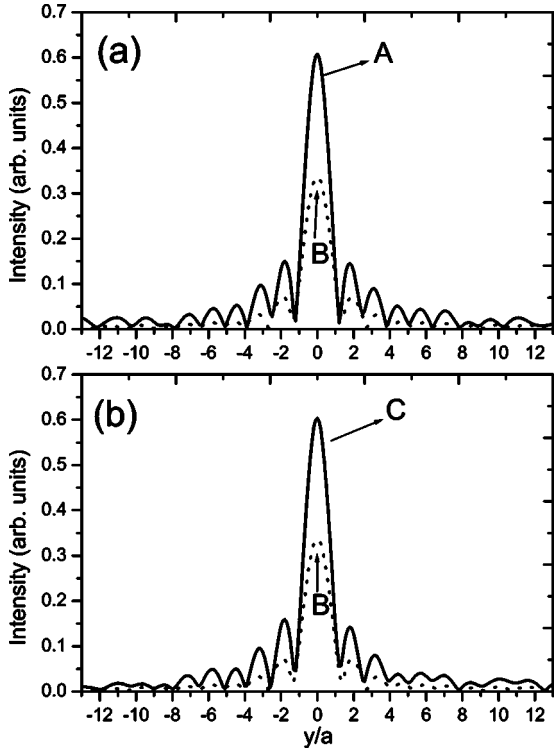

FIG. 11. Intensity distribution along the transverse (y) direction at the image plane for the S wave. (a) The case with absorption (B) and that without absorption (A). (b) The case with absorption (B) and that with absorption and gain (C). The crystal and parameters are identical to those in Fig. 6.

Similar phenomenon can also be found for the P wave. Figures 12(a) and 12(b) show the corresponded case of the P wave. Figure 12(a) represents the intensity distribution as a function of transverse coordinate (y/a) for the P wave at the image plane ($5.5a$ away from the second interface). Comparing curve A without absorption with curve B in the presence of absorption in Fig. 12(a), we find that the absorption decreases the central peak of the image as the case of the S wave. However, with the introducing of gain such as $\epsilon = 7.0 - 0.06i$ for the dielectric part of coated cylinder, the loss due to absorption can be compensated completely. Curve C in Fig. 12(b) represents such a case. In fact, for any cases of absorption, the losses can always be compensated by introducing fitted gain for both polarized waves. Thus, the lens based on the earlier 2D PC can work well even in presence of absorption.

V. SUMMARY

Through the exact numerical simulation and physical analysis, we have demonstrated all-angle single-beam left-handed behavior for both TE and TM modes in the 2D

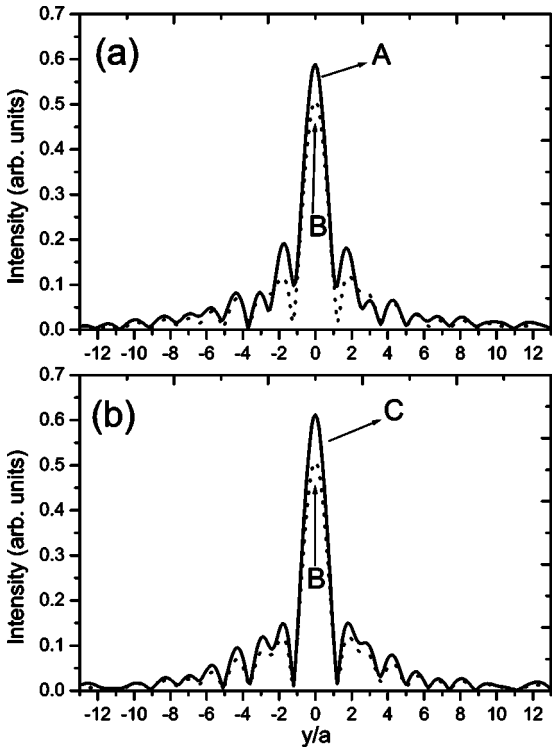

FIG. 12. Intensity distribution along the transverse (y) direction at the image plane for the P wave. (a) The case with absorption (B) and that without absorption (A). (b) The case with absorption (B) and that with absorption and gain (C). The crystal and parameters are identical to those in Fig. 9.

coated photonic crystals. More interestingly, the relative refractive index of −1 for both polarized waves have been found. Furthermore, the refracted angle is linearly proportional to the incident angle in the whole angle region for both polarized waves have been demonstrated. These features are close to the ideal LHM system that can serve as a perfect superlens. The imaging behaviors by 2D coated photonic-crystal-based superlens have been investigated systematically. Good-quality images and focusing, with relative refractive index of −1 and explicitly following the well-known wave-beam negative refraction law, have been observed in these systems for both polarized waves.

Our earlier results are in contrast to the previous investigations about the image behaviors for the LHM-based superlenses and the PC-based microsuperlenses at the lowest valence band. For these cases, the images only appear in the near-field region, which does not follow the rules of geometric optics.[22–27,38,39] According to Pendry's analysis,[5] the perfect image arises from the enhancement of evanescent components of incoming waves, and surface plasmons play an important role in the perfect imaging.[5,21] So, the quality of the image is affected by many factors such as interface feature, finite-size and cavity resonance.[22–27] These will limit further applications. Here, our superlens based on the coated PC systems with triangular lattice can overcome these restrictions. Thus, extensive applications of such a phenomenon to optical devices are anticipated.

In addition, the absorption and compensation for the losses by introducing optical gain in these systems have also been discussed. In general, for the PC structures with metal components, increased absorption in metals prohibits the scaling of these structures to the optical wavelengths. However, since the losses by absorption can always be compensated by introducing fitted gain in our coated PC systems, many negative refraction phenomena that have been observed in the microwave regime can also be found in the optical wavelengths. These features make the PC slabs consisting of coated cylinders promising for application in a range of optical devices, such as a superlens for visible light.

ACKNOWLEDGMENTS

This work was supported by the National Natural Science Foundation of China (Grant No. 10374009) and the National Key Basic Research Special Foundation of China under Grant No. 2001CB610402. The project was sponsored by SRF for ROCS, SEM, and a grant from Beijing Normal University.

[1] V.G. Veselago, Sov. Phys. Usp. **10**, 509 (1968).
[2] J.B. Pendry, A.J. Holden, D.J. Robbins, and W.J. Stewart, IEEE Trans. Microwave Theory Tech. **47**, 2075 (1999).
[3] D.R. Smith, W.J. Padilla, D.C. View, S.C. Nemat-Nasser, and S. Schultz, Phys. Rev. Lett. **84**, 4184 (2000); D.R. Smith and N. Kroll, *ibid.* **84**, 2933 (2000).
[4] R.A. Shelby, D.R. Smith, and S. Schultz, Science **292**, 77 (2001).
[5] J.B. Pendry, Phys. Rev. Lett. **85**, 3966 (2000).
[6] P. Markos and C.M. Soukoulis, Phys. Rev. E **65**, 036622 (2002); Phys. Rev. B **65**, 033401 (2002).
[7] P. Markos, I. Rousochatzakis, and C.M. Soukoulis, Phys. Rev. E **66**, 045601(R) (2002).
[8] R.B. Greegor, C.G. Parazzoli, K. Li, and M.H. Tanielian, Appl. Phys. Lett. **82**, 2356 (2003).
[9] S. Foteinopoulou, E.N. Economou, and C.M. Soukoulis, Phys. Rev. Lett. **90**, 107402 (2003).
[10] J. Pacheco, Jr., T.M. Grzegorczyk, T.B.I. Wu, Y. Zhang, and J.A. Kong, Phys. Rev. Lett. **89**, 257401 (2002).
[11] Y. Zhang, B. Fluegel, and A. Mascarenhas, Phys. Rev. Lett. **91**, 157404 (2003).
[12] D.R. Smith and D. Schurig, Phys. Rev. Lett. **90**, 077405 (2003).
[13] A.A. Houck, J.B. Brock, and I.L. Chuang, Phys. Rev. Lett. **90**, 137401 (2003); C.G. Parazzoli, R.B. Greegor, K. Li, B.E.C. Koltenbah, and M. Tanielian, *ibid.* **90**, 107401 (2003).
[14] J. Li, Lei Zhou, C.T. Chan, and P. Sheng, Phys. Rev. Lett. **90**, 083901 (2003).
[15] R. Ziokowski and E. Heyman, Phys. Rev. E **64**, 056625 (2001).
[16] Focus issue, "Negative refraction and metamaterials," Opt. Express **11**, 7 (2003).
[17] G. Shvets, Phys. Rev. B **67**, 035109 (2003).
[18] V.A. Podolskiy, A.K. Sarychev, and V.M. Shalaev, Opt. Express **11**, 735 (2003).

[19] S.A. Ramakrishna and J.B. Pendry, Phys. Rev. B **67**, 201101(R) (2003).
[20] A.A. Zharov, I.V. Shadrivov, and Y.S. Kivshar, Phys. Rev. Lett. **91**, 037401 (2003); V.M. Agranovich, Y.R. Shen, R.H. Baughman, and A.A. Zakhidov, Phys. Rev. B **69**, 165112 (2004).
[21] G.W. 't Hooft, Phys. Rev. Lett. **87**, 249701 (2001); J.M. Williams, *ibid.* **87**, 249703 (2001); N. Garcia and M. Nieto-Vesperinas, *ibid.* **88**, 207403 (2002); A.L. Pokrovsky and A.L. Efros, *ibid.* **89**, 093901 (2002).
[22] R. Merlin, Appl. Phys. Lett. **84**, 1290 (2004).
[23] L. Chen, S. He, and L. Shen, Phys. Rev. Lett. **92**, 107404 (2004).
[24] D.R. Smith, D. Schurig, J.J. Mock, P. Kolinko, and P. Rye, Appl. Phys. Lett. **84**, 2244 (2004).
[25] Z. Liu, N. Fang, T.-J. Yen, and X. Zhang, Appl. Phys. Lett. **83**, 5184 (2003).
[26] A. Grbic and G.V. Eleftheriades, Phys. Rev. Lett. **92**, 117403 (2004).
[27] A.N. Lagarkov and V.N. Kissel, Phys. Rev. Lett. **92**, 077401 (2004).
[28] H. Kosaka, T. Kawashima, A. Tomita, M. Notomi, T. Tamamura, T. Sato, and S. Kawakami, Phys. Rev. B **58**, R10 096 (1998).
[29] M. Notomi, Phys. Rev. B **62**, 10 696 (2000).
[30] B. Gralak, S. Enoch, and G. Tayeb, J. Opt. Soc. Am. A **17**, 1012 (2000).
[31] S. Foteinopoulou and C.M. Soukoulis, Phys. Rev. B **67**, 235107 (2003).
[32] P.V. Parimi, W.T. Lu, P. Vodo, J. Sokoloff, J.S. Derov, and S. Sridhar, Phys. Rev. Lett. **92**, 127401 (2004).
[33] C. Luo, S.G. Johnson, J.D. Joannopoulos, and J.B. Pendry, Phys. Rev. B **65**, 201104(R) (2002); Opt. Express **11**, 746 (2003); C. Luo, S.G. Johnson, and J.D. Joannopoulos, Appl. Phys. Lett. **83**, 2352 (2002).
[34] E. Cubukcu, K. Aydin, E. Ozbay, S. Foteinopoulou, and C.M. Soukoulis, Nature (London) **423**, 604 (2003).
[35] P.V. Parimi, W.T. Lu, P. Vodo, and S. Sridhar, Nature (London) **426**, 404 (2003).
[36] E. Cubukcu, K. Aydin, E. Ozbay, S. Foteinopoulou, and C.M. Soukoulis, Phys. Rev. Lett. **91**, 207401 (2003).
[37] X. Zhang, Phys. Rev. B **70**, 205102 (2004).
[38] C. Luo, S.G. Johnson, J.D. Joannopoulos, and J.B. Pendry, Phys. Rev. B **68**, 045115 (2003).
[39] Z.Y. Li and L.L. Lin, Phys. Rev. B **68**, 245110 (2003).
[40] J.D. Joannopolous, R.D. Meade, and J.N. Winn, *Photonic Crystals* (Princeton University Press, Princeton, NJ, 1995).
[41] M.M. Sigalas, C.T. Chan, K.M. Ho, and C.M. Soukoulis, Phys. Rev. B **52**, 11 744 (1995); L.M. Li, Z.Q. Zhang, and X. Zhang, *ibid.* **58**, 15 589 (1998).
[42] L.M. Li and Z.Q. Zhang, Phys. Rev. B **58**, 9587 (1998); X. Zhang, Z.Q. Zhang, L.M. Li, C. Jin, D. Zhang, B. Man, and B. Cheng, *ibid.* **61**, 1892 (2000).
[43] D. Felbacq and R. Smaali, Phys. Rev. Lett. **92**, 193902 (2004).